Eng.Research Bull.
Faculty of Eng. & Tech.,
Menoufia University.
Vol. VIII Part II, 1986.
PP: 115-127.

PERFORMANCE OF A DEVELOPED SEGMENTAL ROTOR RELUCTANCE MOTOR

BY

A.M. Osheiba , A.S. Abdel-Karim, and A.A. Hassanien.

Faculty of Eng. & Technology,
Menoufia University,
Shebin El-Koom, EGYPT.

ABSTRACT

In this paper, a developed design for segmental rotor reluctance motor is presented. A self-starting segmental rotor with no cage winding and of higher power to inertia ratio is built and tested. Calculated and experimental results are reported and compared with those of a conventional segmental rotor design. Conditions affecting pole - slipping during starting are studied. Also, the effects of rotor shape and position on the motor current waveform are examined. The reported results show that, the proposed rotor design provides for reduced no load current, higher efficiency, negligible harmonic distortion in the supply current and lower number of pole-slipping during starting.

LIST OF MAIN SYMBOLS

n	number of lost steps, harmonic order of inductance components
N	number of stater turns per pole per phase
H	magnetizing force
ℓ	magnetic path length
L	rotor length, inductance
h	thickness of rotor segment
g	air gap length
R_g	mean air gap radius
R_x	mean rotor radius along the d-axis
R_y	mean rotor radius along the q-axis
x	thickness of rotor segment along the d-axis
y	thickness of rotor segment along the q-axis
i	stator current per phase
$2p$	number of poles
μ	permeability of rotor material
μ_o	permeability of free space
ϕ	flux
Ψ	flux linkage
β	pole arc / pole pitch, ratio

1. INTRODUCTION

Rotor designs of reluctance motors used to be of the conventional salient-pole type where the increase in the saliency ratio was effected by increasing the q-axis reluctance as much as possible. In fact, those earlier designs suffered either from complexity in construction or from restrictions to specific utilities.

Lawernson and Agu[1,2] have developed a segmental rotor design of saliency ratio suitable for practical application, but external means or built in cage windings were necessary for successful starting. Design and performance of reluctance motors have been the subject of many papers [1-6], However, little attention was paid to the study of conditions for stepping forward without pole-slipping. Such an operation is of prime importance for possible position control applications requiring motor of high power ratings.

In principle, energy conversion process in reluctance motors is effected by the term $dL/d\theta$, e.g. by the stator inductance modulation due to rotor rotation[7]. The stator inductances are thus of periodically varying manner which, in general, may inject current harmonics into the supply system[8]. To the best of the author's information, such an effect has been overlooked as far as the reluctance motor performance is concerned.

In this paper a segmental rotor with no cage winding and accordingly low inertia is built and tested. The developed rotor is self-starting with reduced number of pole-slipping and with better steady state performance, The presented rotor design is robust, less in cost and of simple construction.

Performance of the proposed design is considered with particular attention to the effect of motor parameters on pole-slipping during starting. Axes reactances are calculated using linear analysis. The effect of inductance modulation due to rotor shaping on the stator current waverform is also considered and test results are reported. It is shown that the stator current waveform is affected by stator connection and rotor angle. In order to show the virtue of the proposed rotor design, its performance is compared with a rotor based on Lawrenson and Agu/2/ proposal using the same stator. Construction of the experimental motors is considered subsequently.

2. CONSTRUCTION OF THE EXPERIMENTAL MOTORS

In order to obtain consistant results, only one stator was employed with each of the two rotors, which were also made of the same material (solid steel). The employed stator is that of a 3-phase, 1/3 H.P., 4-pole, 220/380 V, 50 Hz squirrel cage induction motor. The shapes and dimensions of the two rotors, RT-1 and RT-2, are as shown in Fig. 1.

The rotor RT-1 is based on the proposal due to Lawrenson and Agu/2/; it comprises four segments, the spaces between them are filled with copper and short - circuited on both rotor sides by end rings. The saliency effect is obtained via the four salient poles of the rotor, while the copper cage is necessary for run-up operation.

The proposed rotor RT-2, is having continuous surface, i.e. the outer shape is cylindrical. The saliency effect is then achieved via four channels grooved along the rotor leaving a suitable thickness for the cylindrical surface. That way, a reseved segmental rotor is obtained as shown in Fig. 1-b. This rotor design requires no cage winding, but alternatively, starting and synchronization is based on the principle of solid rotor induction motor due to the effect of the cylindrical surface.

3. EVALUATION OF THE AXES REACTANCES

Due to its construction, the axes reactances of RT-1 can be evaluated using the approach of reference /4/. That approach is applicable without modification and need not be repeated in this paper.

The proposed rotor, RT-2, has a cylindrical surface, i.e. the air-gap is uniform, but due to the inner saliency effect, fluxes are forced to follow paths

having minimum reluctances. It follows that, this arrangement has the effects of reluctance and hysteresis motors combined. Accordingly, the air-gap flux can be calculated in a manner similar to that used for the hysteresis motor [3], Then the axes flux linkages and accordingly the axes reactances are evaluated. For simplicity, linear analysis is applied and also permeability of the stator is assumed to be infinity.

The model used for analysis is that shown in Fig. 1-b; the broken line represents the mean flux path. The flux which is produced by the mmf (Ni), crosses the air-gap radially and is assumed to be uniformly distributed over the angle θ. Mean cross sectional areas for flux path are taken along the radial direction. Hence, the ampere-turns for the complete magnetic path can be expressed as,

$$Ni = \Sigma H.\ell \tag{1}$$

Following the simplifications made for analysis, the total ampere-turns are given by,

$$2 \int_{o}^{\theta} \frac{1}{\mu} \frac{\phi R_{rm}}{h.L} d\theta + \frac{1}{\mu_o} \cdot \frac{2g}{R_g L} \frac{d\phi}{d\theta} = Ni \tag{2}$$

Equation (2), can be reduced to the form;

$$\alpha_1^2 \lambda(\theta) + \alpha_2^2 \frac{\partial^2}{\partial\theta^2} \lambda(\theta) = \tfrac{1}{2} Ni \tag{3}$$

where

$$\alpha_1 = (R_{rm} / \mu hL)^{\frac{1}{2}} \; ; \quad \alpha_2 = (g/\mu_o R_g L)^{\frac{1}{2}} \text{ and } \lambda(\theta) = \int_{o}^{\theta} \phi \, d\theta .$$

A general solution for equation (3), is easily obtained, from which the rate of change of the airgap flux with respect to the angle θ is given by,

$$\frac{\partial\phi}{\partial\theta} = \frac{Ni}{2\alpha_1\alpha_2} \frac{e^{\alpha(\theta-\pi/2p)} + e^{-\alpha(\theta-\pi/2p)}}{e^{\alpha\pi/2p} + e^{-\alpha\pi/2p}} \tag{4}$$

The flux linkage is related to the flux by;

$$\frac{\partial\Psi}{\partial\theta} = N \frac{\partial\phi}{\partial\theta} \tag{5}$$

The solution given by equation (4) is valid for either of the two rotor positions such that,

$$\alpha = \begin{cases} \alpha_d = \left(\frac{\mu_o}{\mu} \frac{R_x}{X} \frac{R_g}{g}\right)^{\frac{1}{2}} & \text{for } 0 \le \theta \le \frac{\beta\pi}{2p} \; ; \\ \alpha_q = \left(\frac{\mu_o}{\mu} \frac{R_y}{y} \frac{R_g}{g}\right)^{\frac{1}{2}} & \text{for } \frac{\beta\pi}{2p} \le\theta\le \frac{\pi}{2p} \; . \end{cases} \tag{6}$$

$$\alpha_{1d} = (R_x/\mu XL)^{\frac{1}{2}} \; ; \quad \alpha_{1q} = (R_y/\mu yL)^{\frac{1}{2}} \text{ and } \alpha_{2d} = \alpha_{2q} = (g/\mu_o R_g L)^{\frac{1}{2}} \tag{7}$$

Axes Flux Linkages

Considering the solution above, the d-and q-axes flux linkages are expressed as;

$$\Psi_d = \frac{N^2 \, i_d}{2\alpha_{1d}\,\alpha_{2d}} \int_0^{\beta\pi/2p} \frac{e^{\alpha_d(\theta-\pi/2p)} + e^{-\alpha_d(\theta-\pi/2p)}}{e^{\alpha_d \pi/2p} + e^{-\alpha_d \pi/2p}} \, d\theta \; ;$$

and

$$\Psi_q = \frac{N^2 \, i_q}{2\alpha_{1q}\,\alpha_{2q}} \int_{\beta\pi/2p}^{\pi/2p} \frac{e^{\alpha_q(\theta-\pi/2p)} + e^{-\alpha_q(\theta-\pi/2p)}}{e^{\alpha_q \pi/2p} + e^{-\alpha_q \pi/2p}} \, d\theta \; . \qquad (8)$$

Axes Reactances

From equation (5), and carrying out the integration, the d-and q-axes inductances are obtained as;

$$L_d = \frac{\Psi_d}{i_d} = \frac{N^2}{C} \; \frac{e^{\alpha_d(\beta-1)\pi/2p} - e^{-\alpha_d(\beta-1)\pi/2p} + e^{\alpha_d\pi/2p} - e^{-\alpha_d\pi/2p}}{e^{\alpha_d\pi/2p} + e^{-\alpha_d\pi/2p}} \; ,$$

$$L_q = \frac{\Psi_q}{i_q} = \frac{N^2}{D} \; \frac{e^{\alpha_q(1-\beta)\pi/2p} - e^{-\alpha_q(1-\beta)\pi/2p}}{e^{\alpha_q\pi/2p} + e^{-\alpha_q\pi/2p}} \; ,$$

where

$$C = \frac{2}{L}\left(\frac{R_x}{X}\,\frac{g}{R_g}\,\frac{1}{\mu\,\mu_o}\right)^{\frac{1}{2}} \; , \qquad \text{and} \qquad D = \frac{2}{L}\left(\frac{R_y}{y}\,\frac{g}{R_g}\,\frac{1}{\mu\,\mu_o}\right)^{\frac{1}{2}} .$$

The results obtained experimentally and theoretically are listed in Table 1. The measured axes reactances of both rotors were obtained using the method presented in reference (4).

Table 1.

Saturated values of X_d and X_q for both rotors

Rotor type	X_d (Ω)		X_q (Ω)	
	Comp.	Test	Comp.	Test
RT - 1	60	57	37	31
RT - 2	270	258	112	101

Notice that the axes reactances of RT-1 are much less than those of RT-2. Such behaviour is due to the high saturation factor encountered with RT-1, which is not the case with RT-2. The experimental saturation factors for both rotors are 1.53 for RT-1 and 1.21 for RT-2. The measured no-load currents for both rotors at rated voltage are 1.32 A for RT-1 and 0.6 A for RT-2.

4. SYNCHRONOUS PERFORMANCE

The steady-state synchronous performance of the two rotors was evaluated experimentally and predicted theoretically at the rated voltage and frequency.

Summary of the results is listed in table 2, which gives the performance at both full-load and pull-out conditions; full-load is taken as 2/3 of the pull-out power. Machine parameters are listed in Appendix 1.

Table 2.

Results summary of synchronous performance for both rotor types

Performance parameter	RT - 1		RT - 2	
	Computed	Measured	Computed	Measured
$I_{f.L}$, Amp.	2.6	2.2	1.2	1.1
$T_{f.L}$, N-m	2.7	2.4	2.2	2.05
$\eta_{f.L}$	0.28	0.25	0.76	0.72
$\cos \phi_{f.L}$	0.45	0.42	0.62	0.60
I_{max} , Amp.	3.2	2.8	1.38	1.22
T_{max} , N-m	3.6	3.2	2.8	2.4
η_{max}	0.3	0.27	0.78	0.75
$\cos \phi_{max}$	0.52	0.49	0.67	0.64
δ_{max} , ele. deg.	22	20	39.3	39

5. STEPPING-UP PERFORMANCE

If reluctance motors can be made to step satisfactorily, they may provide a relatively cheap powerful stepper; but of course this can only be justified if the phenomenon of lost steps is avoided. In other words, if the supply is switched-on for a certain number of cycles, the rotor should step forward a definite angle determined by the number of excitation cycles. In which case, the machine can be used for stepped position control applications. In this section, a particular attention is paid concerning the range of machine parameters and operating conditions under which the machine will not pole-slip when started from rest. The definition and criterion of lost steps would be found in reference /5/, while the machine equations are taken from reference /6/. Those were put in a state variable form, and conveniently solved numerically using the Runge-Kutta 4 th order method of numerical integration. Parameters used in computation are listed in Appendix 1. The dynamic behaviour of the two prototypes were computed, subject to initial switching angle of α=0 (i.e. the voltage of phase A is zero going positive). To study the starting performance, tests were conducted considering different initial conditions. However, Figs. (2,3) show the variation of speed and load angle for the two models. For RT-1 an unstable operation prevails in which the machine is not able to synchronise at all (Fig. 2); continuous increase of the load angle (dotted curve) of Fig.(3) is shown. In regard to RT-2, the machine successfuly synchronises (Fig.2) with only two lost steps as shown by the solid curve of Fig. (3).

The number of lost steps(n) can be calculated/6/ via predicting the dynamic load angle δ_v during starting period from the following expression:

$$n = \frac{\delta_v - \delta_{vs}}{180} \qquad (10)$$

δ_{vs} is the steady-state load angle necessary to produce steady electromagnetic torque balancing load torque.

The number of lost steps was evaluated assuming direct-switching to the supply (α=0); when motor parameters and supply conditions were unchanged. A comparison results between the two motor models are given in tables (3 through 7). For instance table (6) shows that n = 2 for RT-2 and 17 for RT-1 through 0.5 sec. Notice that in each case only parameter under consideration was varied, whilst the rest of motor parameters were kept unchanged.

Table (3)

Effect of motor inertia, J

J		0.8 J_R	0.6 J_R	0.4 J_R	0.2 J_R
RT - 2	n	2	1	1	0
RT - 1	n	17	15	3	1

Table (4)

Effect of stator resistance, R_a

R_a		0.8 R_a	0.6 R_a	0.4 R_a	0.2 R_a
RT - 2	n	2	3	2	2
RT - 1	n	18	18	19	6

Table (5)

Effect of supply frequency, f

f (Hz)		40	30	20	10	5	2
RT - 2	n	1	*	0	0	0	0
RT - 1	n	14	4	2	1	1	1

* unstable operation.

Table (6)

Effect of initial switching angle, α

α(degree)		0	30	60	90	120	150	180
RT - 2	n	2	3	3	4	4	4	3
RT - 1	n	17	17	15	17	18	18	18

Table (7)

Effect of V/f ratio

V/f		1	2	3
RT - 2	n	2	0	0
RT - 1	n	17	1	0

6. EFFECT OF ROTOR SHAPE ON MOTOR PERFORMANCE

Consider an energised reluctance motor in the steady state. The magnetic circuit of each stator coil would be subjected to a periodic reluctance variation, the waveshape of which is determined by rotor shaping. Due to this saliency effect, the stator coils undergo periodic variations in their inductances, the minimum of which is L_q and the maximum is L_d; the periodic variation is at a fundamental frequency of double that of the supply. This action of inductance modulation due to rotor rotation is a must for energy conversion process in this type of machine.

Fig. 4 is a simplified representation for inductance modulation by the effect of a rotating segmental rotor, where only the fundamental component is shown. As far as the rotor is running in synchronism with the stator, the inductance variation can be expressed as an indpendent function of time. If the stator frequency is ω_1, the periodic variation of a stator coil inductance may be represented in a fourier series as;

$$L(\omega_1 t) = \sum_{n=0}^{\infty} L_n \cos(2n\omega_1 t + \gamma_n) \qquad (11)$$

n is an integer, and the angle(γ_n) signifies the effect of rotor angle. The sinusoidal supply voltage may be expressed as;

$$V(\omega_1 t) = V_m \sin(\omega_1 t + \phi) \qquad (12)$$

where ϕ is the phase shift between $V(\omega_1 t)$ and the fundamental current $i_1(t)$. The current flowing in the modulated inductance will, in general, contain components of all possible modulation frequencies /8/, e.g. $(2n\omega_1 \pm \omega_1)$.

The resulting current components may be written as,

$$i(\omega_1 t) = I_1 \sin \omega_1 t + \sum_{n=1}^{\infty} I_k \sin[(1+2n)\omega_1 t + \phi_k] \qquad (13)$$

Quantitative analysis of the harmonic current components is quite difficult, but their effects can be discussed on the light of equations, and above. For instance, the input power to a stator phase is given by,

$$P = \frac{1}{2\pi} \int_0^{2\pi} V(\omega_1 t)\, i(\omega_1 t)\, d\omega_1 t \qquad (14)$$

This gives,

$$P = \tfrac{1}{2} V_m I_1 \cos\phi \quad \text{for } k = 1$$
$$= \text{zero} \quad \text{for } k \neq 1 \qquad (15)$$

That is to say, only the fundamental current I_1 can contribute to the input power to the motor. In general, the machine power factor is determined as,

$$\lambda = \frac{P}{VI} = \frac{I_1}{\sqrt{2}\ I} \text{ Cos } \phi \qquad (16)$$

$$\sqrt{2}\ I = \sqrt{\sum_{n=0}^{\infty} I_k^2} \qquad > I_1 \qquad (17)$$

It follows that, the higher the harmonic currents the lower the machine power factor at the same input power. Also, the harmonic current components contribute to stator losses and produce undesirable harmonic torques due to distorsion of flux waveform. This results in reduction in the machine efficiency.

The above undesirable effects can be eliminated by taking care of the rotor shape and stator connection as follows. If the rotor is shaped such that reluctance of the magnetic circuit is made to vary at only the frequency $2w_1$, e.g. equation (11) becomes,

$$L\ (\omega_1 t) = L_o + L_1 \text{ Cos } (2\omega_1 t + \gamma_1) \qquad (18)$$

Referring to equation (13), the resulting current would then become,

$$i\ (\omega_1 t) = I_1 \text{ Sin } \omega_1 t + I_3 \text{ Sin } (3\omega_1 t + \phi_3) \qquad (19)$$

Thus, a star-connected stator with isolated neutral would cause elimination of the third harmonic current leaving only the fundamental component. The experimental current waveforms shown in Fig. 5, indicate clearly that the developed rotor (RT-2) satisfies the above requirements, which are also reflected on the overall performance as reported before, The conventional segmental rotor, however, suffers from the current distorsion which would also affect the mains supply.

7. CONCLUSIONS

Performance of a developed segmental rotor reluctance motor has been studied and compared with one of a conventional design. Theoretical and experimental results have shown that the proposed rotor design provides for higher power to inertia ratio, higher efficiency, reduced no load current and higher power factor. They have also shown that the proposed rotor shape reduces distorsion in the rotor current and if the stator is star-connected with isolated neutral the motor current becomes nearly sinusoidal.

The study of stepping up and starting performance has shown that, due to its low inertia, the proposed design can be started without pole-slipping if the supply frequency is below 20 Hz. It also required less time to pull into synchronism. Based on the study of pole-slipping phenomenon, the use of the proposed design as a powerful stepper is feasible.

8. REFERENCES

[1] Lawrenson, P.J. and Agu, L.A., "Theory and performance of polyphase Reluctance Machines", Proc. IEEE, Vol. 111, No. 8, Aug. 1964, PP. 1435-1445.

[2] Lawrenson, P.J. and Agu, L.A., "Low-intertia Reluctance Machines", Proc. IEE, Vol. 111, No. 12, Dec. 1964, PP. 2017-2025.

[3] Rahman, M.A. and Osheiba, A.M., "Steady-State Performance Analysis of Polyphase Hysteresis-Reluctance Motors", IEEE Trans. on Industry Applications, Vol. IA-12, No. 4, May/June 1985, PP. 659-663.

[4] Hassan, S.A., Osheiba, A.M. and Mohamedin, A.L., "A Generalized Approach for the Evaluation of Reluctance Motor Reactances", Electric Machines and Electromechanies, Vol. 5, No. 2, 1980, pp. 155-168, USA.

[5] Stephenson, J.M., Hughes, A and Hassanein, A.A.: "Synchronisation of reluctance motor without pole slipping". Proc., IEE conference, London, Sept. 1981, U.K.

[6] Hassan, S.A., Hassanien, A.A. and Mohamedein, A.L., "Effect of Parameter Variations on pole slipping for Reluctance Motors", Electric Machines and Power Systems, Vol. 10, No. 1, pp. 53-65, 1985, USA.

[7] White, D.C. and Woodson, H.H. "Electromechanical energy conversion" Wiley, 1959.

[8] Tucker, D.G. "Circuits with time varying parameters", J. Brit. I.R.E., Vol. 25, p. 263, March, 1963.

Appendix. 1

Machine Parameters

	R_a	X_d	X_q	X_{md}	X_{mq}	$X\ell_{2d}$	$X\ell_{2q}$
RT - 1	27	51	31	29	9	41	50.6
RT - 2	27	258	102	236	80	101	110
	$X\ell_1$	X_{2d}	X_{2q}	R_{2d}	R_{2q}	2P	J
RT - 1	22	70	59.6	18.3	50.6	4	0.00112
RT - 2	22	337	190	78.3	89	4	0.00092

All resistances and reactances in ohms and J in kg - m^2.

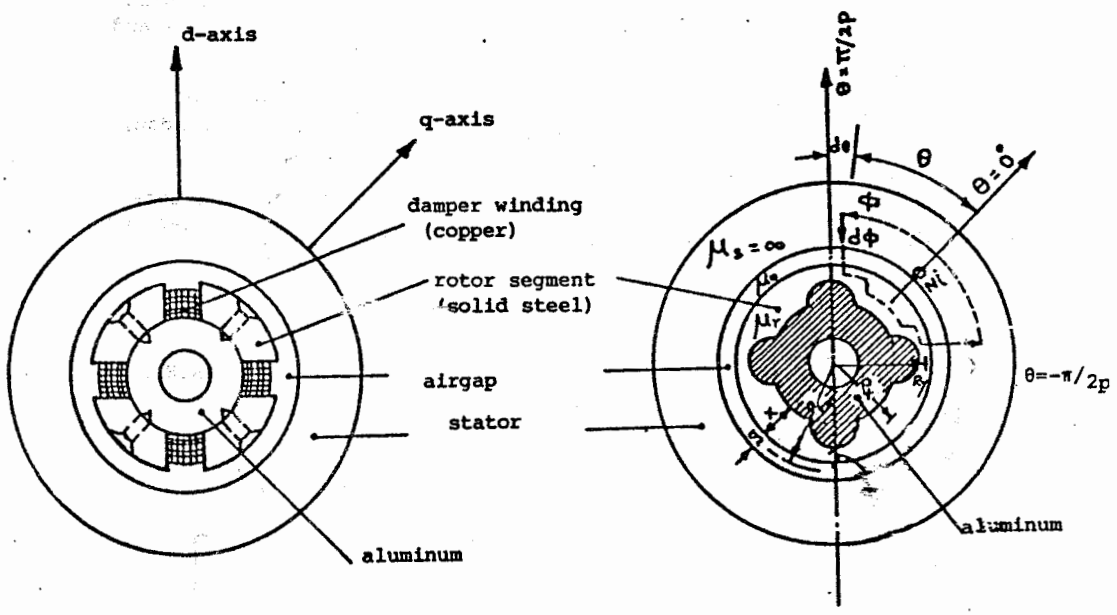

a) Rotor RT-1 .

b) Rotor RT-2..

Fig. 1 : Configurations of experimental rotors.

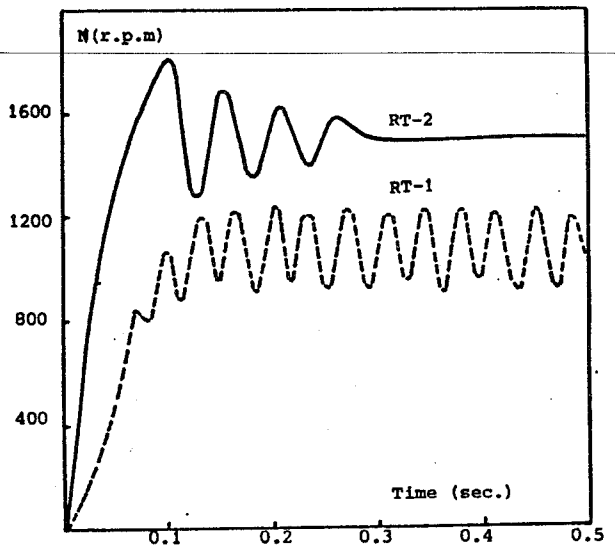

Fig. 2: Speed - time characteristics at f = 50 H_z and $\alpha = 0°$.

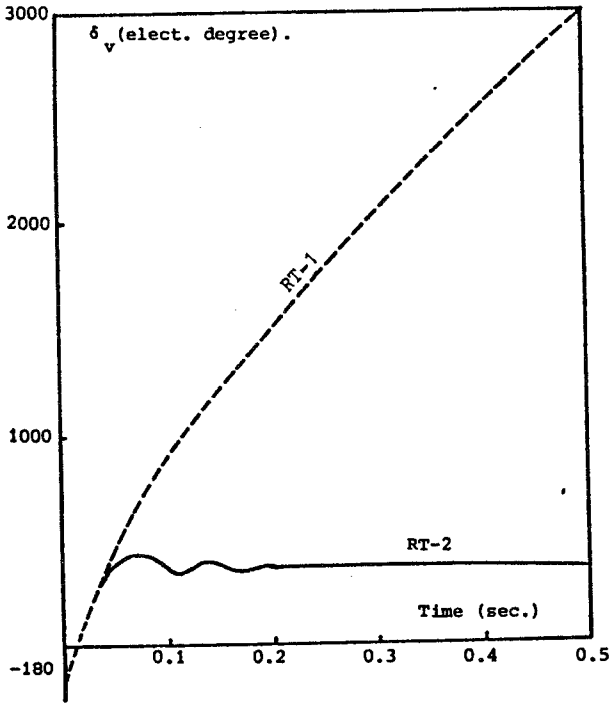

Fig. 3: Load angle-time characteristic at f=50 H_z and $\alpha=0°$.

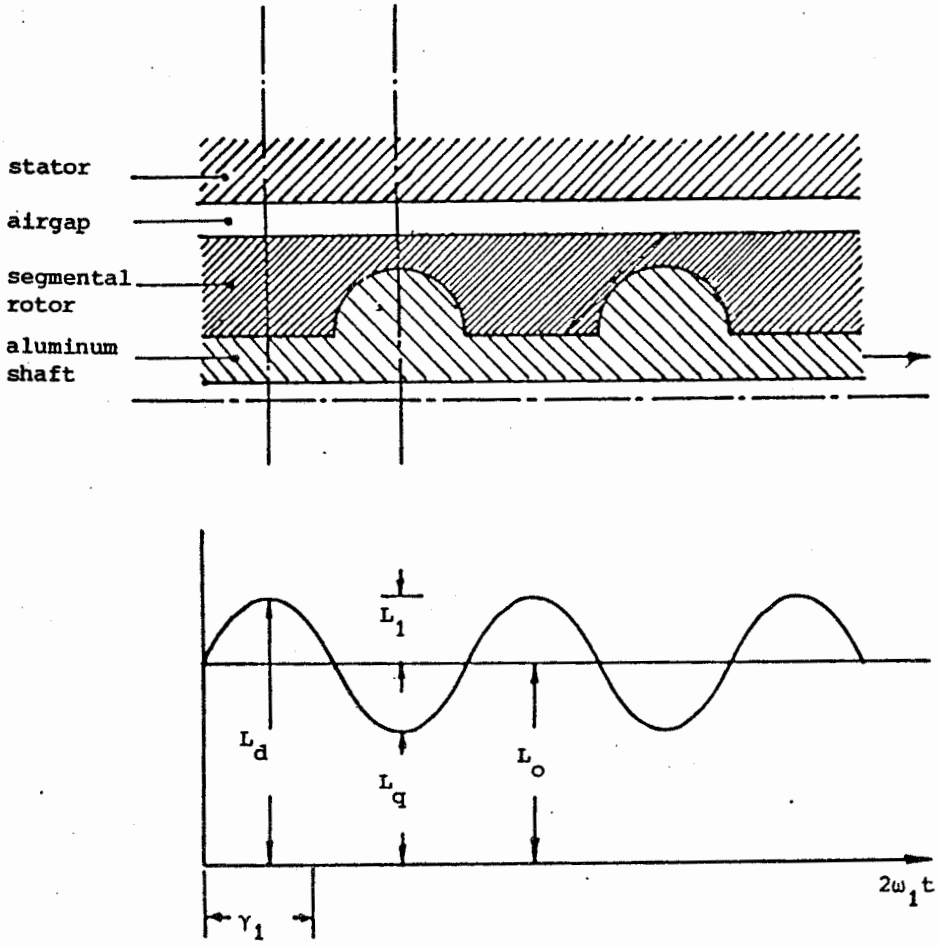

Fig. 4: Fundamental component variation of the stator inductance.

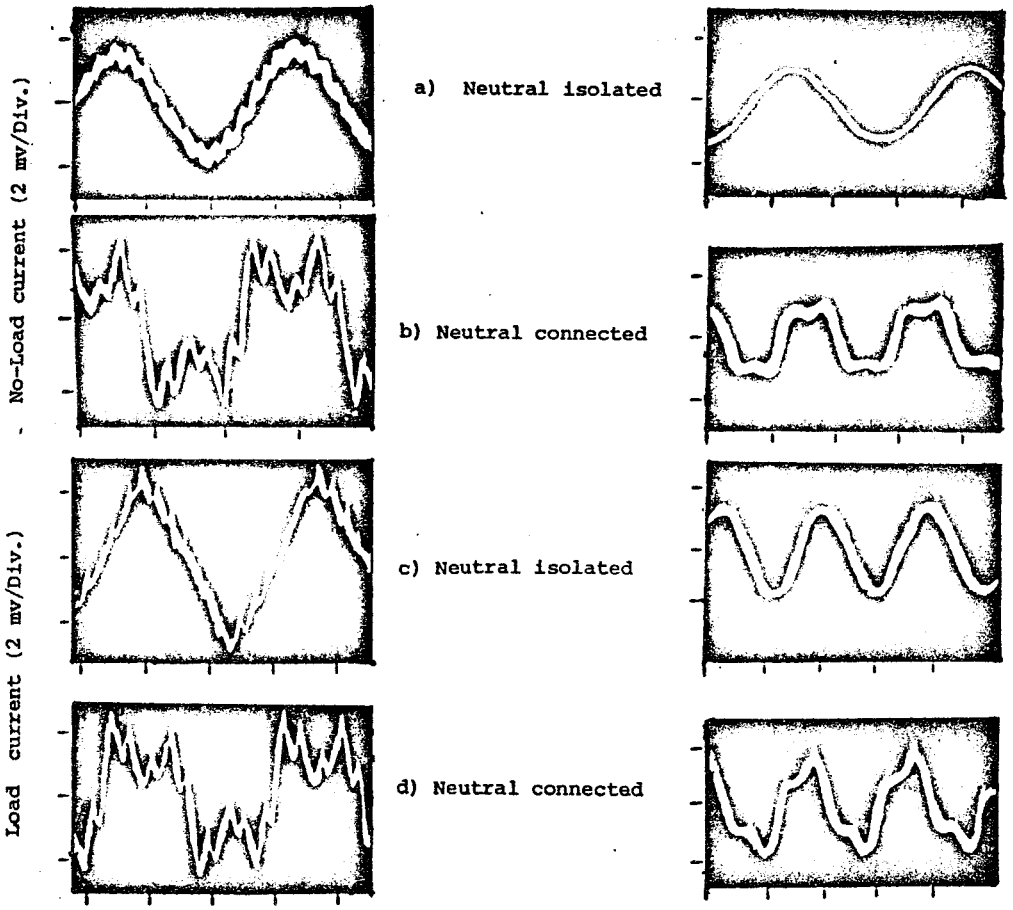

Fig. 5: Oscillograms of stator current waveforms under different conditions.